Macromolecules

pubs.acs.org/Macromolecules Article

Molecular-Weight Dependence of Center-of-Mass Chain Diffusion in Polymerized Ionic Liquid Melts

Peng Lan, Qiujie Zhao, Guangxin Lv, Grant S. Sheridan, David G. Cahill, and Christopher M. Evans*

Cite This: *Macromolecules* 2023, 56, 3383−3392 Read Online

ACCESS | Metrics & More | Article Recommendations | Supporting Information

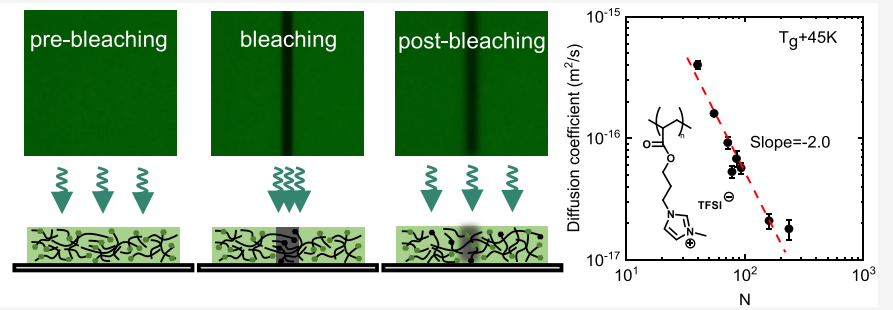

ABSTRACT: Polymerized ionic liquids (PILs) with flexible polymer chains and weakly interacting ionic liquid (IL) groups have received great attention for their desirable properties in electrochemical applications such as ionic conductivity. Less is known about their dynamic properties such as center-of-mass chain diffusion and how it depends on molecular weight in the presence of IL groups. In this work, a series of acrylic PILs with imidazolium cations and bis(trifluoromethanesulfonyl)imide (TFSI) anions (TFSI-f-PIL$_N$) were synthesized via reversible addition−fragmentation chain-transfer polymerization with degrees of polymerization N ranging from 40 to 236. A fluorescent acrylic monomer with the 7-nitrobenzofurazan group was copolymerized at trace levels as a probe of chain motion, and the diffusion coefficient (D) of TFSI-f-PIL$_N$ was determined by fluorescence recovery after photo bleaching at T_g + 45 K. Within the uncertainty of 3−20%, a scaling relationship of $D \sim N^{-2}$ was observed which is the same as the scaling of linear neutral polymers. Wide-angle X-ray scattering exhibited no peak at ∼5 nm^{-1}, indicating no long-range imidazolium-TFSI ionic correlations. Our results indicate that the molecular weight dependence of center-of-mass diffusion is not affected by electrostatic interactions of IL groups. No transition from a Rouse regime ($D \sim N^{-1}$) to reptation regime ($D \sim N^{-2}$) was observed within the studied N range.

INTRODUCTION

Polymerized ionic liquids (PILs) are a class of ionic polymers with bulky, weakly interacting ionic liquid groups (IL) covalently attached to the polymer backbone. They exhibit good thermal stability, electrochemical stability, moderate single-ion conductivity, and tunable mechanical properties, which makes them promising functional polymer materials for applications like energy storage and conversion,[1,2] stimuli-responsive materials,[3] and separation membranes.[4] As a model system, linear PILs with varying counterion groups,[5] sidechain chemistry,[6,7] copolymer composition,[8,9] IL placement,[10] ionic content,[11] and molecular weight[12−14] have been studied to uncover their structure−properties relationships. Studies have determined free ion mobility,[15−17] static dielectric constant[18] and how conductivity can decouple from segmental relaxation.[19−21] Simulation efforts have also provided key insights into how the nanostructure affects PIL properties.[22−25] While a majority of the studies on PILs focus on understanding ion conduction, other dynamic properties such as viscosity and center-of-mass chain diffusion are also important in the context of processing, 3D printing,[26] electrode wetting,[27] and tunable electro-adhesion.[28] The diffusion coefficient of polymer chains and its chain length dependence are of critical importance when considering transference numbers, where ion−polyion correlations exist and the motion of a highly charged polymer chain can still contribute to conductivity in PILs.[29]

A limited number of experimental results for viscosity scaling in PILs have been previously reported.[12,13,30,31] In a work by Fan et al.,[30] acrylic ammonium bis(trifluoromethanesulfonyl)-imide (TFSI) PILs showed a viscosity scaling of $\eta \sim M^{1.1}$, concluding that ion interactions play only a minor role on the scaling relation. In a separate work by Nakamura et al.,[13] power law factors of $\eta \sim M^{1.7}$ to $\eta \sim M^{4.2}$ were reported for the unentangled and entangled regimes, and the higher-than-

Received: November 23, 2022
Revised: March 24, 2023
Published: April 28, 2023

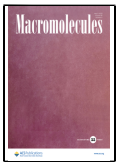

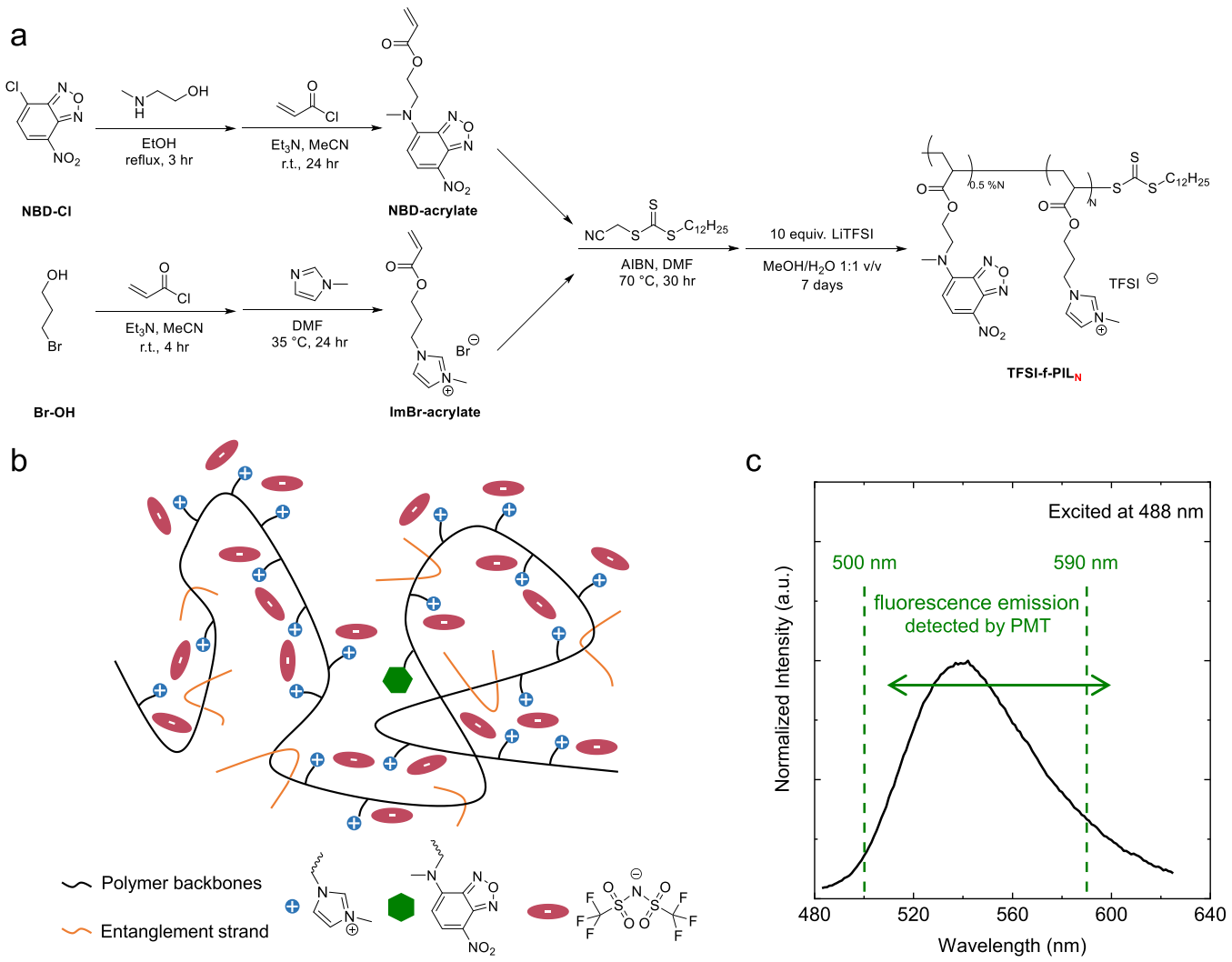

Figure 1. (a) Synthesis route of TFSI-f-PIL$_N$ using RAFT polymerization for precise control of degree of polymerization N, which is calculated by the end-group analysis of the NMR spectra of TFSI-f-PIL$_N$. (b) Molecular structure of TFSI-f-PIL$_N$ with fluorescence dye (NBD-acrylate) randomly attached to the polymer backbone as a probe for FRAP measurement. (c) Representative fluorescence emission spectra of TFSI-f-PIL$_N$ (N = 42). The detection wavelength for FRAP measurement ranges from 500 to 590 nm and PMT are used in confocal microscope to detect the fluorescence signal.

expected values were attributed to the existence of strong electrostatic interaction between IL groups. A broadening of the complex modulus in the glass-to-rubber transition regime was observed and the degree of broadening showed a molecular weight dependence.[13] In a follow-up study, they attributed this to internal torsional motions or sub-rouse modes where interchain interactions were reduced by ionized large counterions.[32] Recent work from our group[12] reported scaling of $\eta \sim M^{1.0}$ to $\eta \sim M^{2.3}$, in agreement with Fan et al.[30] as well as Rouse model prediction ($\eta \sim M^{1.0}$) for unentangled polymers. Both Fan et al.[30] and Zhao and Evans[12] did not observe a broadening of complex modulus which could be due to the longer spacing of the ionic groups from the backbone in the present work (propyl acrylate spacer rather than a direct linkage to the backbone), leading to greater mobility of the ionic groups. This may also be related to the difference in scaling exponents found in the different studies.

The most widely applied theory for the chain dynamics of linear polymer melts is the reptation model, where the chain motion of entangled neutral polymers is described as diffusing along its contour constrained by neighbor chains.[33] The model predicts that the diffusion coefficient D scales with degree of polymerization (N) as

$$D \sim \frac{kT}{\zeta} \cdot \frac{N_e}{N^2} \tag{1}$$

where N_e denotes an entanglement strand containing N_e monomers, ζ is the friction factor. This theory is consistent with experimental[34−36] and computational results[37,38] for various neutral polymer melts. It has been pointed out that deviations from this theoretical scaling law can occur due to factors like contour length fluctuation (CLF)[39−42] which may impact viscosity and diffusion coefficient differently because of the different time scales involved. Frischknecht and Milner have noted that the molecular weight dependence of diffusion shifts from $D \sim M^{-2.25}$ to $D \sim M^{-2.0}$ when N/N_e is larger than 80,[42] as CLF becomes less important in longer chains. Lodge have reported the $D \sim M^{-2.4\pm0.1}$ behavior for polybutadiene melts within the whole range of molecular weights studied,[34] concluding that the effect of CLF in diffusion dynamics is comparable to that in viscosity measurements.

https://doi.org/10.1021/acs.macromol.2c02388
Macromolecules 2023, 56, 3383−3392

To the best of our knowledge, no studies have probed how the molecular weight scaling of polymer diffusion coefficients in PILs are affected by the IL groups along the backbone. Chain dynamics in ionomers are typically discussed using the sticky Rouse model where additional constraints on chain motion are imposed by associating ion pairs.[43] The ion pairs act as stickers and N_s is denoted as the degree of polymerization per sticker (in the case of PILs, $N_s = 1$), and the reptation model can be modified as

$$D \sim \frac{kT}{\zeta} \cdot \frac{N_e}{N^2} \cdot \frac{N_s^2 \tau}{\tau_s} \quad (2)$$

where τ is the relaxation time of a monomer (diffuses a distance of an order of the monomer size) and τ_s is the lifetime of associating ion pairs. Such a theory applied in studies of polystyrene ionomers[44,45] and polyether ionomers,[46] but in the case of PILs, the ionic interactions are substantially weaker. Nevertheless, eq 2 suggests that ionic interactions should affect the absolute value of D but not its molecular weight dependence, assuming τ_s and τ do not depend on N. Although difficult to quantify, the number of "free" ions which are dissociated at any given point in time is ~0.1% of the total content, as reported from dielectric spectroscopy analysis[5] and surface force measurements.[47] Nevertheless, this number is not expected to be molecular weight-dependent once the polymer is entangled. Tests of how ionic interactions and aggregation affect D in PILs of different molecular weight are currently lacking.

To measure chain diffusion in polymers, methods including pulse field gradient NMR,[35,48] secondary ion mass spectroscopy,[49] small-angle neutron scattering,[50] fluorescence recovery after photobleaching (FRAP),[51] and forward recoil spectrometry (FRS)[36] have been employed. FRAP is used in the present work because of the relative ease of attaching a fluorescence label and detection using a microscope. FRAP has been widely used in probing small molecule diffusion in polymer melts,[52] polymer diffusion in solution/multilayer film,[53] bio-macromolecules in membranes,[54] and dense polymer melts.[55,56]

In this work, the center-of-mass diffusion of PILs were probed using FRAP. A series of fluorescence-labeled PILs with the increase in number-averaged degree of polymerization (N) and imidazolium TFSI groups (TFSI-f-PIL$_N$) were synthesized by reversible addition−fragmentation chain-transfer polymerization (RAFT) with narrow dispersity $Đ < 1.20$. Self-diffusion coefficients were measured combining FRAP post-bleaching images and diffusion fitting models. Experimental errors were estimated by uncertainty contours to validate the diffusion fitting model. The measured diffusion coefficient scaling was $D \sim N^{-2.0}$, which agreed well with the scaling predicted by entangled neutral polymers, indicating that the interaction of IL groups do not affect the N dependence of diffusion in the PILs studied. No transition from Rouse regime ($D \sim N^{-1}$) to reptation regime ($D \sim N^{-2}$) was observed. The morphology of TFSI-f-PIL$_N$ from wide-angle X-ray scattering (WAXS) also showed no low q ion aggregates peaks compared to similar IL monomer, indicating the electrostatic interaction is too weak to form significant intercluster ionic aggregates.

EXPERIMENTAL SECTION

Synthesis of Fluorescent Poly[methylimidazolium Bis-(trifluoromethanesulfonyl)imide Propyl Acrylate]. The synthesis route of TFSI-f-PIL$_N$ is shown in Figure 1a and details are shown in the Supporting Information. The synthesis of fluorescent dye from a chloro-7-nitrobenzofurazan (NBD-Cl) precursor to NBD-modified acrylate monomer is similar to previous work with slight modifications.[55] The imidazolium-bromide acrylate monomers (ImBr-acrylate) were synthesized from 3-bromopropanol (Br−OH) via a facile reaction with acryloyl chloride, followed by quaternization with 1-methyl imidazole. The precise control of molecular weight was achieved through RAFT and NBD acrylate was attached to polymer chains through copolymerization. Finally, TFSI-f-PIL$_N$ were formed through ion exchange using 10 equiv of LiTFSI. The molecular structure of TFSI-f-PIL$_N$ is shown in Figure 1b.

Nuclear Magnetic Resonance. Synthesis of the products NBD-acrylate and ImBr-acrylate was confirmed by NMR measured at room temperature using a U500 or UI500NB spectrometer. Number-averaged molecular weight (M_n) of TFSI-f-PIL$_N$ was determined by end-group analysis based on the baseline and phase-corrected NMR spectra of TFSI-f-PIL$_N$ in DMSO-d_6. The integration of CH_3 protons (3H per chain, 0.8−0.9 ppm) on the RAFT chain end was set to be 3, and the integration of imidazolium protons (1H per repeat unit, ~9 ppm) directly gave the degree of polymerization N in TFSI-f-PIL$_N$ (Figure S1).

Size-Exclusion Chromatography. The polydispersity of TFSI-f-PIL$_N$ was determined using a Tosoh EcoSEC Elite Model HLC-8420, equipped with two Tosoh TSKgel Alpha-M columns, and a Tosoh Dual-Flow refractive index (RI) detector. Because the fluorescent samples (TFSI-f-PIL$_N$) saturate the light scattering detector which is equipped with a 504 nm green laser, only the RI detector was used to determine the polydispersity in this work. The elution solvent was a mixture of water, methanol, and acetic acid (54:23:23 v/v/v) with 0.54 M sodium acetate (measured pH = 4.15), which was previously reported for molecular weight determination of ionenes[57] and PILs with similar IL groups in our previous work.[12] The mixture was vacuum filtered with two layers of 0.22 μm Nylon membrane filters (Thomas Scientific) and used for elution and sample preparation. The polymers were dissolved at 50 °C for at least 6 h and filtered through 0.45 μm Nylon or Teflon syringe filters (Fisher Scientific). The sample concentrations were 1−3 mg/mL and the injection volumes were 50 μL. The sample flow rate was 0.6 mL/min and the column temperature was 50 °C. A dispersity poly(ethylene oxide) (PEO) standard (20.9 kDa, $Đ$ = 1.04, PolyAnalytik) was used for detector calibration and elution time correction. A Dextran standard (74.8 kDa, $Đ$ = 1.31, PolyAnalytik) was used for molecular weight validation. For conventional calibration, Br-anion PILs with the same backbone and cations (Br-PIL, 8 samples with M_n = 14−85 kDa) but without fluorescent labels were used as "standards" via light scattering. Br-PILs were also dissolved and eluted using the conditions described above. The data were processed by Tosoh SECview software and we constructed a calibration curve using the non-fluorescent versions of Br PILs with known M_p values. This calibration curve was then applied to the fluorescent TFSI-f-PILs.

Thermal Characterization. The thermal transitions of TFSI-f-PIL$_N$ were measured by differential scanning calorimetery (TA2500 DSC instrument) using Hermetic pan with a 10 °C/min heating/cooling rate from −50 to 150 °C (Figure S2). The T_g versus N relationship was fitted into the Fox−Flory equation (Figure S3).

UV−Visible Light Absorption Spectroscopy. NBD-acrylate was dissolved in methanol at different concentrations to prepare a series of UV−vis calibration standards. TFSI-f-PIL$_N$ were also dissolved in methanol with known polymer concentrations. The solution was loaded into a quartz cuvette (Hellma Analytics, optical path length = 1 cm) and the absorption spectrum (Figure S4) was collected using a Varian Cary 5G UV−vis spectrometer at room temperature with nitrogen purging. The absorbance at 472 nm was used to construct the calibration curve (Figure S5) and to calculate the fluorescence dye concentration in TFSI-f-PIL$_N$ based on the Lambert−Beer Law (Figure S6).

Fluorescence Spectroscopy. The fluorescence emission spectra of TFSI-f-PIL$_N$ were collected using a Horiba PTI QM-400 fluorometer equipped with a 75 W halogen lamp at excitation wavelength = 488 nm (Figure 1c). The polymer was sandwiched between a glass slide and a coverslip and loaded onto the fluorometer.

https://doi.org/10.1021/acs.macromol.2c02388
Macromolecules 2023, 56, 3383−3392

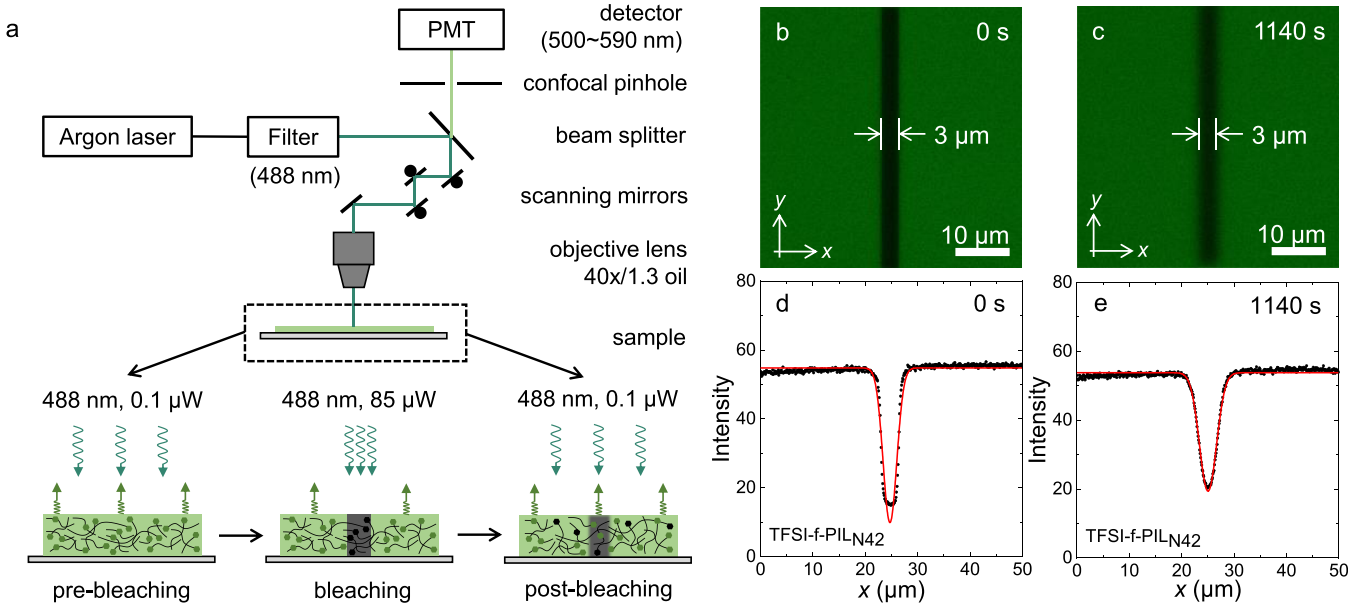

Figure 2. (a) Schematic of FRAP measurement. Low intensity argon laser (488 nm, 0.1 μW) was used to excite the fluorescence emission of the dye molecule, which was detected by the PMT detector in a confocal microscope (ranges from 500 to 590 nm). High intensity laser (488 nm, 85 μW) was used for bleaching the dye molecule in a defined bleaching region and post-bleaching images were captured every minute. (b) Bleaching fluorescence image of TFSI-f-PIL$_{N42}$ at 30 °C (T_g + 45 K) (t = 0 s). The bleached region is 3 μm × 50 μm. Image size is 50 μm × 50 μm with an array of 512 × 512 pixels. (c) Post-bleaching fluorescence image of TFSI-f-PIL$_{N42}$ at t = 1140 s. (d) Averaged fluorescence intensity profile of bleaching image as a function of x position (black dots). The red solid line is the fitted Gaussian function. (e) Averaged fluorescence intensity profile of post-bleaching image at t = 1140 s as a function of x position (black dots). The red solid line is the fitted Gaussian function.

The excitation and emission slit widths were 1 nm. The acquisition step size was 1 nm and the integration time was 1 s per step.

Sample Preparation for FRAP. Sample preparation was performed in the Argon glovebox to minimize the oxygen-induced self-quenching of the fluorescence dye molecule. About 5 mg of TFSI-f-PIL$_N$ was added on top of a glass slide and annealed at 60 °C for 10 min to remove trapped gas bubbles. It was then covered by a coverslip and pressed by a weight of 0.5 kg at 60 °C for another 10 min to get a sandwiched sample of homogeneous thickness (~0.2 mm). The four edges of cover slip were sealed by epoxy sealant (Devcon 2 Ton Epoxy) before taken out of the glovebox to avoid oxygen and moisture.

Self-Diffusion Coefficient Measurements. The self-diffusion dynamics of the TFSI-f-PIL$_N$ was characterized using FRAP on a Leica SP8 confocal laser scanning microscope equipped with an UNO incubation system (Okolab) for temperature control (the schematic is shown in Figure 2a). All microscope operation was controlled by Leica LAS X software. The samples were equilibrated at 30 °C (T_g + 45 K) for 15 min before FRAP. The images were captured using a 40× oil immersion objective (NA = 1.3) and the zoom in factor was 5.81 to give a region of interest (ROI) of 50 μm × 50 μm with an array of 512 × 512 pixels. The scanning speed was 1000 Hz. The excitation wavelength was 488 nm, generated by an Argon laser (65 mW, output power was set to be 60%), and the pre/post-bleach scanning power was set at 0.1−0.2% of the output power. The actual incident laser power targeted at the sample was measured using a power meter (Newport model 1918-C with detector 818-SL) and the actual pre/post-bleach scanning power was measured to be 0.1 μW. The gain of the photomultiplier tube (PMT) detector was set at 600−650 V with detection wavelength ranging from 500 to 590 nm. The samples were bleached in a defined rectangular region of 3 μm × 50 μm at the center for 2.5 s with bleaching power set at 100% of the output power using the same laser as pre/post-bleach scanning (actual incident power = 85 μW). The bleaching region was achieved by changing the angle and position of three galvanometric scanning mirrors in the microscope. The $1/e^2$ attenuation length of the incident laser was ~30 μm. The post-bleached images were taken every minute and each of them was converted to a matrix of fluorescence intensities with intensity readout between 0 and 255.

X-ray Scattering. The morphology of the TFSI-f-PIL$_N$ was characterized by transmission WAXS and small-angle X-ray scattering (SAXS). The setup was composed of a Xenocs GeniX3D Cu Kα X-ray source (1.54 Å) and a Pilatus 2D detector. Samples were inserted into capillary tubes made of quartz (1.5 mm, Hilgenberg) and annealed at 60 °C for 24 h. The sample-to-detector distance was calibrated with silver behenate prior to the measurement and WAXS/SAXS spectra were recorded with a 30 min exposure time at room temperature. FIT2D software was used for processing and integrating the 2-D scattering patterns.

RESULTS AND DISCUSSION

In Situ PIL Self-Diffusion Measurement Using Fluorescence Recovery after Photobleaching. The self-diffusion of TFSI-f-PIL$_N$ is measured by FRAP and analyzed using Fick's second law

$$\frac{\partial C}{\partial t} = D\left(\frac{\partial^2 C}{\partial^2 x} + \frac{\partial^2 C}{\partial^2 y} + \frac{\partial^2 C}{\partial^2 z}\right) \tag{3}$$

where C represents the concentration of diffusing species under consideration and D is the diffusion coefficient. In our experiment, fluorescent dye molecules (NBD acrylate) are randomly attached to the polymer chains at trace levels to track the transport behavior of TFSI-f-PIL$_N$ (Figure 1b). Some will occur at chain ends and others at various points along the backbone. Therefore, the concentration of diffusing polymer chains is proportional to the concentration of fluorescence dye molecules, which can be quantified by the fluorescence intensity under the microscope. The use of a label requires that the attached dye molecules will not affect the diffusion behavior of bulk polymer and we minimized the effect by controlling the dye content to be 0.5 mol % per chain

https://doi.org/10.1021/acs.macromol.2c02388
Macromolecules 2023, 56, 3383−3392

(approximately one dye molecule per polymer chain). For the simplicity of experiments, a single line (3 μm × 50 μm) is bleached at the center of the medium (Figure 2b), and during a time lapse, polymer chains from unbleached region will gradually diffuse to the bleached center (in x direction) due to Brownian motion (Figure 2c). We exclude the section at the top/bottom periphery of post-bleaching images because there is also y-direction diffusion at the edge of bleached region. Therefore, the diffusion behavior of TFSI-f-PIL$_N$ in our FRAP measurement can be simplified as a one-dimension diffusion with infinite extended boundary and its solution is written as

$$C(x, t) = \frac{M_{\text{diffuse}}}{2(\pi Dt)^{1/2}} e^{-(x-x_0)^2/4Dt} \tag{4}$$

Here, M_{diffuse} denotes the total amount of fluorescence dye molecules per unit length in the x direction and x_0 is the center of bleached region (x_0 = 25 μm in our case). The concentration profile of fluorescence dye at different times can be quantified as intensity signals in each post-bleaching image, which can be fitted into Gaussian function (as shown in Figure 2d,e)[58]

$$\begin{aligned} I(x, t) &= I_0 - \frac{M_{\text{diffuse}}}{2(\pi Dt)^{1/2}} e^{-(x-x_0)^2/4Dt} \\ &= I_0 - A(t) e^{-(x-x_0)^2/2w^2} \end{aligned} \tag{5}$$

where I represents the fluorescence intensity at position x and time t after bleaching, M_{diffuse} is the fluorescence intensity (per unit length in x direction) corresponding to the amount of fluorophore destroyed by bleaching, and w is the full width at half-maximum (FWHM) of the fitted Gaussian function. Comparison of the exponential term gives the following linear fitting function

$$w^2 = 2Dt \tag{6}$$

Therefore, by plotting w^2 as a function of time t for a series of fluorescence intensity profiles obtained from post-bleaching images, a linear fitting line with a slope of 2D passing through the origin can be obtained. With the increase in time, the intensity curve is broadened and FWHM increases.

In a FRAP experiment, the bleached region at t = 0 s is characterized by a finite width (3 μm in our case) rather than an infinitely sharp line of an ideal initial condition, and the bleaching time is set to be 2.5 s rather than an infinitely short time pulse and this was sufficient to bleach out 70% of the initial fluorescent intensity. Model corrections for these deviations either on the length scale or time scale have been considered (Figure S7)

$$w^2 = 2Dt + w_0^2 = 2D(t + t_0) \tag{7}$$

where w_0 is the FWHM at t = 0 s, which can also be transformed to a shift in time, time lag t_0, obtained by extrapolating the fitted line to w^2 = 0. It should be noted that this shift in length scale or time scale does not impact the determination of diffusion coefficient, which comes from the slope of the data.

Measurement errors typically come from experimental errors and systematic errors. Systematic errors are examined by simulating the FRAP diffusion problem based on Fick's second law. The initial condition is chosen as the fluorescent intensity profile of the postbleaching image when t = 0 s (in Figure 2d), which has a near-Gauss shape due to laser intensity distribution. The PDE problem is solved and the overall fluorescent intensity profile is generated as a function of x position and postbleaching time t (Figure S8). The first is to validate the boundary condition in FRAP experiment for Gauss fitting, as the ROI (5×10^{-5} m) is considered to be infinite boundary. For the simulated post-bleaching time (2 h), the as-obtained total amount of fluorescent intensity (the integral of the fitting Gauss function) remains constant to satisfy mass balance, which suggests that the selected ROI the boundary could be treated as infinite boundary for Gauss fitting. The second is to examine the systematic error in the linear fitting of w^2 versus t due to experimental limits of short total post-bleaching time. In comparison of experimental data, linear fitting of simulated w^2 versus t is plotted in Figure S9 and both results agree well with the slope of 2D, which indicates there is no systematic error in the linear fitting even when changes of w^2 is small.

Experimental errors are estimated based on the goodness-of-fitting between experiment and model data sets. Deviations of the measured $w_{e,i}^2$ from the values predicted by linear fitting model are calculated as follows

$$\sigma_e = \sum_i^k (w_{e,i}^2 - w_{m,i}^2)^2 \tag{8}$$

where $w_{e,i}$ is the FWHM in the fluorescence intensity profile obtained from FRAP experiments, $w_{m,i}$ is predicted by linear fitting model $w_{m,i}^2 = 2D(t + t_0)$, and i is the number index of post-bleaching images. The uncertainty contour of diffusion coefficient and time lag are defined when deviation satisfies (the confidence level is 95%)

$$\frac{\sigma}{\sigma_e} = 2 \tag{9}$$

An example of uncertainty contour of diffusion coefficient and time lag for TFSI-f-PIL$_{42}$ are marked by the red circle region in Figure S10, where the minimum deviation σ_{min} is at the center of the contour and the experimental error is calculated by comparing the diffusion coefficient at σ_{min} and at $2\sigma_{\text{min}}$.

Results of the linear fitting for the FRAP measurement of TFSI-f-PIL$_N$ are shown in Figure 3a and from the uncertainty contour of diffusion coefficient and time lag (Figure 3b), the uncertainty of fitting for different samples vary from 3 to 20%. Typically, higher N samples show larger experimental errors and we attribute this to the fact that higher N samples have lower diffusion coefficient and are more likely to be affected by drifting of the region of interest. The drifting of ROI in the z-direction can lead to fluctuation of baseline fluorescence intensity, while drifting of ROI in the x-direction can lead to variations in the local self-diffusion. Fitting errors can also come from the fluorescent bleaching process, as the bleaching laser power will heat up the polymers within the bleached region. We hypothesized that the fluctuation of diffusion in the first few post-bleaching images is due to this thermally induced relaxation of polymers.

Diffusion Coefficient Scaling in PILs. The effect of molecular weight on the self-diffusion of TFSI-f-PIL$_N$ is determined by plotting diffusion coefficient versus degree of polymerization obtained from NMR end-group analysis in Figure 4. For comparison, a red dash line with the slope of −2.0 is drawn as a scaling prediction for neutral polymers. The

https://doi.org/10.1021/acs.macromol.2c02388
Macromolecules 2023, 56, 3383−3392

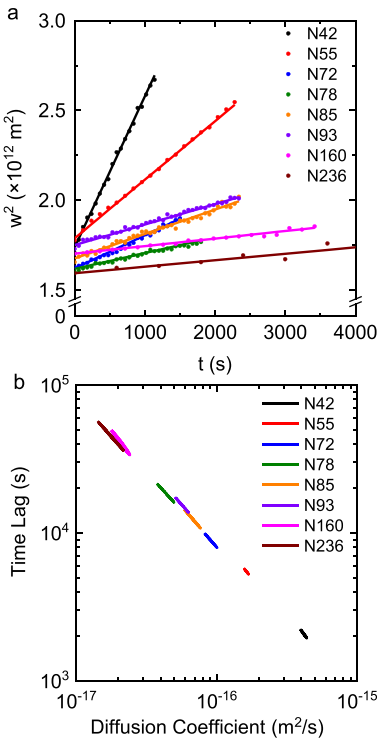

Figure 3. (a) Plots of w^2 as a function of time (t) for TFSI-f-PIL$_N$. The filled dots are extracted from the fitted Gaussian function in fluorescence intensity profile of each post-bleaching image. The solid lines are the fitted linear function with slopes of 2D. Extrapolation of the fitted lines to $w^2 = 0$ yields the time lag t_0. (b) Uncertainty contour of diffusion coefficient D and time lag t_0 for TFSI-f-PIL$_N$. The circle regions are goodness-of-fitting errors and the best fit is at the center of the contour.

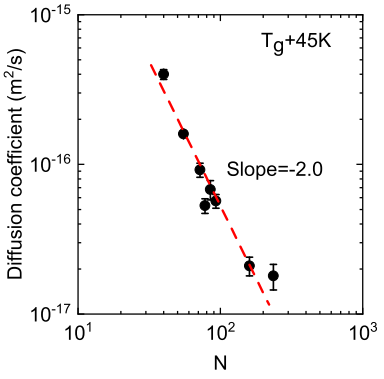

Figure 4. Molecular weight (degree of polymerization, N) dependence of TFSI-f-PIL$_N$ diffusion coefficient (D) at 30 °C (T_g + 45 K). The red dash line with a slope of −2.0 is drawn as a predicted $D \sim N$ scaling from entangled neutral polymers. The error bar of each sample comes from the uncertainty of fitting (Table 1).

absolute values of diffusion coefficient and uncertainty for all samples are shown in Table 1. In general, with the increase in N from 42 to 236, the diffusion coefficient decreases monotonically by an order of magnitude from 4.2×10^{-16} to 1.8×10^{-17} m^2/s and is consistent with the $D \sim N^{-2}$ relationship, which agrees well with the reptation theory.[33] This result indicates that the scaling of chain dynamics of TFSI-f-PIL$_N$ are the same as for entangled neutral polymers, and the presence of ionic interaction does not affect the molecular weight dependence of diffusion coefficient in the PIL studied. In contrast to our previous viscosity scaling results,[12] no transition from Rouse regime ($D \sim N^{-1}$) to reptation regime ($D \sim N^{-2}$) was observed in the PIL samples. Prior scaling analysis of viscosity in neutral polybutadiene indicated a slope of $N^{1.0}$ for N below approximately 37 and $N^{3.4}$ above N = 185.[59] An intermediate, continually varying slope was observed in between these limits, and in the present work, the onset of entanglements is $N \sim 90$ when the onset of a transition regime occurs.[12] Thus, the $D \sim N^{-2}$ scaling occurs even for unentangled PILs as low as N = 42. We estimated the characteristic time scale of diffusion τ_D using the following relation

$$\tau_D = {R_g}^2/D \tag{10}$$

For each sample, the R_g is calculated based on prior work for similar PILs.[60] Using shear rheology data from our previous work,[12] with τ_t, terminal relaxation time was then determined as[61]

$$\tau_t \sim \lim_{\omega \to 0} \frac{G'(\omega)}{\omega G''(\omega)} \tag{11}$$

This corresponds to the longest relaxation, where polymer chains are viscoelastically relaxed and the relaxation mode is simply diffusive. In all cases, τ_D is close to or larger than τ_t, and thus, longer times are required for chain diffusion to experience full relaxation of orientational anisotropy over end-to-end distance then viscosity. This may explain the apparent differences in scaling behavior based on viscosity and diffusion coefficients.

We examined several hypotheses for this single diffusion coefficient scaling regime based on prior computational and experimental studies. First, several works have reported the effect of molecular weight dependence of free volume on the self-diffusion.[35,62] According to the Vogel−Fulcher equation, the friction factor ζ can be related to the reciprocal of fractional free volume which has a temperature-dependent impact on diffusion coefficients. It was reported that diffusion coefficients for polyethylene only showed a $D \sim N^{-2}$ scaling over a broad range of molecular weights.[62] However, after the diffusion data were corrected to have the same free volume (or the same friction), two distinct regimes could be observed corresponding to $D \sim N^{-1}$ and $D \sim N^{-2}$ at the onset of entangled behavior.[62] Simulations also showed the friction coefficient increases from a small value characteristics of short alkanes chains to a chain-length-independent plateau when $N \sim 60-80$.[63] In our TFSI-f-PIL$_N$, from N = 42−236, the glass transition temperature only varies by 5 °C, suggesting that free volume does not change much with the increase in molecular weight. Therefore, it is unlikely free volume is affecting the self-diffusion scaling.

Another factor affecting the flow properties of polymers is the molecular weight distribution, especially when considering constraint release since the rapid motion of short chains releases constraints on longer chains.[64−66] In the simulation work of Peters et al., they studied the diffusion coefficient scaling of polymers with polydispersity from 1.0 to 1.16 and concluded that although shorter chains diffuse faster than longer chains, the polydispersity in that range still did not alter the entanglement time or tube diameter.[67] In this work, the dispersity of TFSI-f-PILN are $Đ \sim 1.3$ (shown in Table 1) based on the RI detector. Without a LS detector, only relative molecular weight can be generated from RI signal, which is

https://doi.org/10.1021/acs.macromol.2c02388
Macromolecules 2023, 56, 3383−3392

Table 1. Summary of the Number-Averaged Molecular Weight ($M_{n(NMR)}$, Measured by NMR End Group Analysis), Number-Averaged Molecular Weight ($M_{n(RI)}$, Measured by RI Detector in GPC), $Đ_{(RI)}$ (Polydispersity Measured by RI Detector in GPC), Glass Transition Temperature (T_g, Measured by DSC), and Self-Diffusion Coefficient of TFSI-f-PIL$_N$ (D, Measured by FRAP)

sample	N	$M_{n(NMR)}$ (kg/mol)	$M_{n(RI)}$ (kg/mol)	$Đ_{(RI)}$	T_g (°C)	$D \times 10^{16}$ (m^2/s)	error bar (%)
TFSI-f-PILN_{42}	42	20.3	23.2	1.32	−17	4.18 ± 0.3	5
TFSI-f-PILN_{55}	55	26.4	27.2	1.35	−16	1.60 ± 0.07	3
TFSI-f-PILN_{72}	72	34.5	34.7	1.37	−15	0.92 ± 0.1	10
TFSI-f-PILN_{78}	78	37.4	36.9	1.30	−14	0.53 ± 0.06	11
TFSI-f-PILN_{85}	85	40.7	38.6	1.36	−16	0.68 ± 0.1	15
TFSI-f-PILN_{93}	93	44.5	40.1	1.33	−15	0.57 ± 0.06	10
TFSI-f-PILN_{160}	160	76.3	72.0	1.31	−13	0.21 ± 0.03	15
TFSI-f-PILN_{236}	236	112.4	102.2	1.40	−12	0.18 ± 0.03	20

more sensitive to the small molecular weight fraction compared with a LS detector. Therefore, the as-measured dispersity by RI is expected to be higher than the actual value of our PILs, which should not qualitatively affect the self-diffusion scaling.

The role of chain flexibility on the scaling of diffusion coefficients has also been considered. Bulacu and van der Giessen studied the effect of semi-flexibility of chains on polymer diffusion and found that increasing bending/torsion rigidity will not only reduce the absolute value of diffusion coefficient but also move the onset of entanglement to longer chains until it becomes undefined.[68] They also found the increased stiffness or decreasing the temperature near T_g will result in a chain length dependence approaching $D \sim N^{-2}$ for both unentangled or mildly entangled chains.[69] Such a power law shift due to temperature decrease for short, neutral polymer chains has also been reported by in simulation and experiments.[70] The present PILs may be effectively stiffer than neutral polymers (silicones, polybutadiene, and acrylates) if the bulky ionic groups affect the conformations of the chain, although still more flexible than the PILs of Nakamura et al.[13] where the ionic group is directly attached to the backbone. Our viscosity values are almost 4 orders of magnitude lower for a given N supporting this idea. In this case, the absence of a transition regime may be rationalized.

The morphology of TFSI-f-PIL$_N$ was also studied using SAXS/WAXS (Figure 5). No peaks are observed in SAXS spectra, indicating the absence of long-range ordered structure in the PILs studied. Based on previous work on the assignment of PIL scattering peaks,[5,71−73] the high q_I peak (~13.5 nm^{-1}) represents the amorphous halo and the intermedium q_{II} peak (~9.2 nm^{-1}) represents the anion−anion correlations. An intercluster ionic aggregate peak q_{III} at ~4−5 nm^{-1} is not observed for imidazolium-TFSI correlations, compared with the same IL monomer[73] or smaller ionic groups (such as BF^{4-}).[5,72] This supports the diffusion coefficient scaling results that the molecular weight dependence of diffusion coefficient is not affected by ion associations or aggregation in the present PILs. With the increase in molecular weight, the correlation peak position remains the same, which indicates that chain length has no discernible effect on the morphology of the PILs in the N range studied.

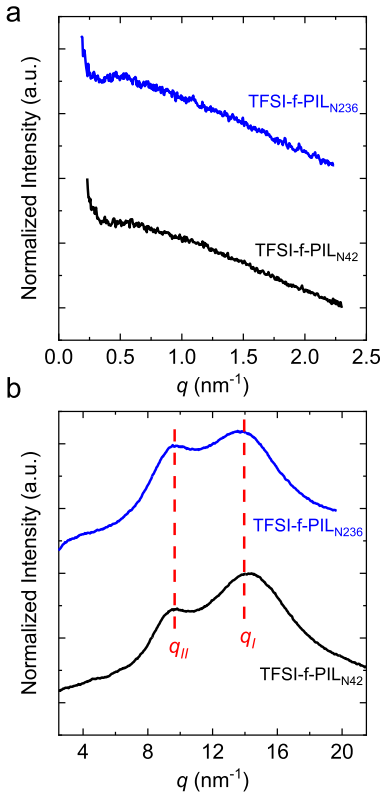

Figure 5. (a) SAXS spectra of TFSI-f-PIL$_{N42}$ (black curve) and TFSI-f-PIL$_{N236}$ (blue curve). No peaks are observed in the SAXS profile. (b) The WAXS spectra of TFSI-f-PIL$_{N42}$ (black curve) and TFSI-f-PIL$_{N236}$ (blue curve). The red dash lines indicate peaks that correspond to the amorphous halo of polymers (q_I, ~14 nm^{-1}), the anion−anion correlation (q_{II}, ~9 nm^{-1}).

CONCLUSIONS

In this work, we systematically studied the effect of degree of polymerization (N = 42−236) on the chain dynamics of linear polyacrylate ionic liquids (TFSI-f-PIL$_N$). FRAP was used to monitor the in situ diffusion behavior of TFSI-f-PIL$_N$ with NBD-acrylate attached to the polymer backbone as fluorescence probe through random copolymerization. It was the first time to use FRAP in studying the macroscopic diffusion behavior of solvent-free, fully charged PILs. The fluorescence intensity profile was analyzed assuming one-dimensional diffusion model and fitted by Gaussian function. Within experimental errors (3−20%), the diffusion coefficient scaling was $D \sim N^{-2.0}$, which agrees well with that of linear neutral polymer in the entangled regime, but no transition from the Rouse regime to reptation regime was observed. We hypothesized that the imidazolium−TFSI interaction will slightly increase the rigidity of polymer chains, but such ionic aggregation or correlations are too weak to affect the molecular weight dependence of diffusion dynamics compared

https://doi.org/10.1021/acs.macromol.2c02388
Macromolecules 2023, 56, 3383−3392

to linear neutral polymers. WAXS spectra also showed no ionic aggregation for the imidazolium−TFSI interactions.

■ ASSOCIATED CONTENT

Supporting Information

The Supporting Information is available free of charge at https://pubs.acs.org/doi/10.1021/acs.macromol.2c02388.

Synthesis route of TFSI-f-PIL$_N$; elemental analysis (F and Br); NMR spectra for end group analysis; DSC heat flow curves; T_g versus N plot; UV−vis absorption of NBD-acrylate; concentration calibration curve of NBD-acrylate; UV−vis absorption of TFSI-f-PIL$_N$ and NBD-acrylate concentration calculation; linear fitting of w^2 versus t; simulated intensity profile as a function of x and t; total amount of bleached intensity in the ROI as a function of t; linear fitting of w^2 versus t based on simulation data ($D = 4.2 \times 10^{-16}$ m^2/s); and uncertainty contour of diffusion coefficient D and time lag t_0 (PDF)

■ AUTHOR INFORMATION

Corresponding Author

Christopher M. Evans − *Department of Materials Science and Engineering, Materials Research Laboratory, and Beckman Institute for Advanced Science and Technology, University of Illinois at Urbana-Champaign, Urbana, Illinois 61801, United States;* orcid.org/0000-0003-0668-2500; Email: cme365@illinois.edu

Authors

Peng Lan − *Department of Chemical and Biomolecular Engineering, University of Illinois at Urbana-Champaign, Urbana, Illinois 61801, United States; Materials Research Laboratory, University of Illinois at Urbana-Champaign, Urbana, Illinois 61801, United States*

Qiujie Zhao − *Department of Materials Science and Engineering and Materials Research Laboratory, University of Illinois at Urbana-Champaign, Urbana, Illinois 61801, United States;* Present Address: Capacitor Sciences Inc., 1530 O'Brien Drive Suite B, Menlo Park, California 94025, United States; orcid.org/0000-0003-1860-8148

Guangxin Lv − *Department of Materials Science and Engineering and Materials Research Laboratory, University of Illinois at Urbana-Champaign, Urbana, Illinois 61801, United States;* orcid.org/0000-0002-7933-4331

Grant S. Sheridan − *Department of Materials Science and Engineering and Materials Research Laboratory, University of Illinois at Urbana-Champaign, Urbana, Illinois 61801, United States*

David G. Cahill − *Department of Materials Science and Engineering and Materials Research Laboratory, University of Illinois at Urbana-Champaign, Urbana, Illinois 61801, United States;* orcid.org/0000-0001-5969-3460

Complete contact information is available at: https://pubs.acs.org/10.1021/acs.macromol.2c02388

Notes

The authors declare no competing financial interest.

■ ACKNOWLEDGMENTS

This work was funded by the National Science Foundation (NSF) under award DMR-1751291. The research was carried out in the Material Research Laboratory (for synthesis, and DSC, WAXS, and UV−vis instrument), the Microanalysis Laboratory (for halide element analysis), NMR Laboratory (for NMR), Beckman Institute for Advanced Science and Technology (for FRAP measurement) at the University of Illinois, Urbana-Champaign. We also thank Dr. Hiroshi Watanabe from Institute for Chemical Research, Kyoto University for providing suggestion for physical interpretation of the diffusion results.

■ REFERENCES

(1) Mecerreyes, D. Polymeric ionic liquids: Broadening the properties and applications of polyelectrolytes. *Prog. Polym. Sci.* **2011**, *36*, 1629−1648.

(2) Shaplov, A. S.; Marcilla, R.; Mecerreyes, D. Recent Advances in Innovative Polymer Electrolytes based on Poly(ionic liquid)s. *Electrochim. Acta* **2015**, *175*, 18−34.

(3) Green, M. D.; Wang, D.; Hemp, S. T.; Choi, J.-H.; Winey, K. I.; Heflin, J. R.; Long, T. E. Synthesis of imidazolium ABA triblock copolymers for electromechanical transducers. *Polymer* **2012**, *53*, 3677−3686.

(4) Bara, J. E.; Hatakeyama, E. S.; Gabriel, C. J.; Zeng, X.; Lessmann, S.; Gin, D. L.; Noble, R. D. Synthesis and light gas separations in cross-linked gemini room temperature ionic liquid polymer membranes. *J. Membr. Sci.* **2008**, *316*, 186−191.

(5) Choi, U. H.; Ye, Y.; Salas de la Cruz, D.; Liu, W.; Winey, K. I.; Elabd, Y. A.; Runt, J.; Colby, R. H. Dielectric and Viscoelastic Responses of Imidazolium-Based Ionomers with Different Counterions and Side Chain Lengths. *Macromolecules* **2014**, *47*, 777−790.

(6) Fan, F.; Wang, Y.; Hong, T.; Heres, M. F.; Saito, T.; Sokolov, A. P. Ion Conduction in Polymerized Ionic Liquids with Different Pendant Groups. *Macromolecules* **2015**, *48*, 4461−4470.

(7) Choi, U. H.; Mittal, A.; Price, T. L.; Gibson, H. W.; Runt, J.; Colby, R. H. Polymerized Ionic Liquids with Enhanced Static Dielectric Constants. *Macromolecules* **2013**, *46*, 1175−1186.

(8) Weber, R. L.; Ye, Y.; Schmitt, A. L.; Banik, S. M.; Elabd, Y. A.; Mahanthappa, M. K. Effect of Nanoscale Morphology on the Conductivity of Polymerized Ionic Liquid Block Copolymers. *Macromolecules* **2011**, *44*, 5727−5735.

(9) Chen, H.; Choi, J.-H.; Salas-de la Cruz, D.; Winey, K. I.; Elabd, Y. A. Polymerized Ionic Liquids: The Effect of Random Copolymer Composition on Ion Conduction. *Macromolecules* **2009**, *42*, 4809−4816.

(10) Kuray, P.; Noda, T.; Matsumoto, A.; Iacob, C.; Inoue, T.; Hickner, M. A.; Runt, J. Ion Transport in Pendant and Backbone Polymerized Ionic Liquids. *Macromolecules* **2019**, *52*, 6438−6448.

(11) Nakamura, K.; Saiwaki, T.; Fukao, K. Dielectric Relaxation Behavior of Polymerized Ionic Liquid. *Macromolecules* **2010**, *43*, 6092−6098.

(12) Zhao, Q.; Evans, C. M. Effect of Molecular Weight on Viscosity Scaling and Ion Transport in Linear Polymerized Ionic Liquids. *Macromolecules* **2021**, *54*, 3395−3404.

(13) Nakamura, K.; Saiwaki, T.; Fukao, K.; Inoue, T. Viscoelastic Behavior of the Polymerized Ionic Liquid Poly(1-ethyl-3-vinylimidazolium bis(trifluoromethanesulfonylimide)). *Macromolecules* **2011**, *44*, 7719−7726.

(14) Keith, J. R.; Mogurampelly, S.; Aldukhi, F.; Wheatle, B. K.; Ganesan, V. Influence of molecular weight on ion-transport properties of polymeric ionic liquids. *Phys. Chem. Chem. Phys.* **2017**, *19*, 29134−29145.

(15) Kisliuk, A.; Bocharova, V.; Popov, I.; Gainaru, C.; Sokolov, A. P. Fundamental parameters governing ion conductivity in polymer electrolytes. *Electrochim. Acta* **2019**, *299*, 191−196.

(16) Cheng, Y.; Yang, J.; Hung, J.-H.; Patra, T. K.; Simmons, D. S. Design Rules for Highly Conductive Polymeric Ionic Liquids from Molecular Dynamics Simulations. *Macromolecules* **2018**, *51*, 6630−6644.

(17) Stacy, E. W.; Gainaru, C. P.; Gobet, M.; Wojnarowska, Z.; Bocharova, V.; Greenbaum, S. G.; Sokolov, A. P. Fundamental

Limitations of Ionic Conductivity in Polymerized Ionic Liquids. *Macromolecules* **2018**, *51*, 8637−8645.
(18) Choi, U. H.; Mittal, A.; Price, T. L.; Lee, M.; Gibson, H. W.; Runt, J.; Colby, R. H. Molecular Volume Effects on the Dynamics of Polymerized Ionic Liquids and their Monomers. *Electrochim. Acta* **2015**, *175*, 55−61.
(19) Wang, Y.; Agapov, A. L.; Fan, F.; Hong, K.; Yu, X.; Mays, J.; Sokolov, A. P. Decoupling of Ionic Transport from Segmental Relaxation in Polymer Electrolytes. *Phys. Rev. Lett.* **2012**, *108*, 088303.
(20) Jones, S. D.; Nguyen, H.; Richardson, P. M.; Chen, Y.-Q.; Wyckoff, K. E.; Hawker, C. J.; Clément, R. J.; Fredrickson, G. H.; Segalman, R. A. Design of Polymeric Zwitterionic Solid Electrolytes with Superionic Lithium Transport. *ACS Cent. Sci.* **2022**, *8*, 169−175.
(21) Agapov, A. L.; Sokolov, A. P. Decoupling Ionic Conductivity from Structural Relaxation: A Way to Solid Polymer Electrolytes? *Macromolecules* **2011**, *44*, 4410−4414.
(22) Wheatle, B. K.; Lynd, N. A.; Ganesan, V. Correction to "Effect of Polymer Polarity on Ion Transport: A Competition between Ion Aggregation and Polymer Segmental Dynamics". *ACS Macro Lett.* **2019**, *8*, 947.
(23) Wheatle, B. K.; Keith, J. R.; Mogurampelly, S.; Lynd, N. A.; Ganesan, V. Influence of Dielectric Constant on Ionic Transport in Polyether-Based Electrolytes. *ACS Macro Lett.* **2017**, *6*, 1362−1367.
(24) Ganesan, V. Ion transport in polymeric ionic liquids: recent developments and open questions. *Mol. Syst. Des. Eng.* **2019**, *4*, 280−293.
(25) Zhang, Z.; Wheatle, B. K.; Krajniak, J.; Keith, J. R.; Ganesan, V. Ion Mobilities, Transference Numbers, and Inverse Haven Ratios of Polymeric Ionic Liquids. *ACS Macro Lett.* **2020**, *9*, 84−89.
(26) Schultz, A. R.; Lambert, P. M.; Chartrain, N. A.; Ruohoniemi, D. M.; Zhang, Z.; Jangu, C.; Zhang, M.; Williams, C. B.; Long, T. E. 3D Printing Phosphonium Ionic Liquid Networks with Mask Projection Microstereolithography. *ACS Macro Lett.* **2014**, *3*, 1205−1209.
(27) Liu, J.; Selvan, M. E.; Cui, S.; Edwards, B. J.; Keffer, D. J.; Steele, W. V. Molecular-Level Modeling of the Structure and Wetting of Electrode/Electrolyte Interfaces in Hydrogen Fuel Cells. *J. Phys. Chem. C* **2008**, *112*, 1985−1993.
(28) Kim, H. J.; Paquin, L.; Barney, C. W.; So, S.; Chen, B.; Suo, Z.; Crosby, A. J.; Hayward, R. C. Low-Voltage Reversible Electroadhesion of Ionoelastomer Junctions. *Adv. Mater.* **2020**, *32*, 2000600.
(29) Fong, K. D.; Self, J.; McCloskey, B. D.; Persson, K. A. Onsager Transport Coefficients and Transference Numbers in Polyelectrolyte Solutions and Polymerized Ionic Liquids. *Macromolecules* **2020**, *53*, 9503−9512.
(30) Fan, F.; Wang, W.; Holt, A. P.; Feng, H.; Uhrig, D.; Lu, X.; Hong, T.; Wang, Y.; Kang, N.-G.; Mays, J.; Sokolov, A. P. Effect of Molecular Weight on the Ion Transport Mechanism in Polymerized Ionic Liquids. *Macromolecules* **2016**, *49*, 4557−4570.
(31) Wieland, F.; Bocharova, V.; Münzner, P.; Hiller, W.; Sakrowski, R.; Sternemann, C.; Böhmer, R.; Sokolov, A. P.; Gainaru, C. Structure and dynamics of short-chain polymerized ionic liquids. *J. Chem. Phys.* **2019**, *151*, 034903.
(32) Inoue, T.; Matsumoto, A.; Nakamura, K. Dynamic Viscoelasticity and Birefringence of Poly(ionic liquids) in the Vicinity of Glass Transition Zone. *Macromolecules* **2013**, *46*, 6104−6109.
(33) de Gennes, P. G. Reptation of a Polymer Chain in the Presence of Fixed Obstacles. *J. Chem. Phys.* **1971**, *55*, 572−579.
(34) Lodge, T. P. Reconciliation of the Molecular Weight Dependence of Diffusion and Viscosity in Entangled Polymers. *Phys. Rev. Lett.* **1999**, *83*, 3218−3221.
(35) Bachus, R.; Kimmich, R. Molecular Weight and Temperature Dependence of Self-diffusion Coefficients in Polyethylene and Polystyrene Melts Investigated Using a Modified n.m.r. Field-Gradient Technique. *Polymer* **1983**, *24*, 964−970.
(36) Mills, P. J.; Green, P. F.; Palmstro/m, C. J.; Mayer, J. W.; Kramer, E. J. Analysis of diffusion in polymers by forward recoil spectrometry. *Appl. Phys. Lett.* **1984**, *45*, 957−959.
(37) Rubinstein, M. Discretized model of entangled-polymer dynamics. *Phys. Rev. Lett.* **1987**, *59*, 1946−1949.
(38) Hagita, K.; Takano, H. Self-diffusion of a polymer chain in a melt. *J. Phys. Soc. Jpn.* **2003**, *72*, 1824−1827.
(39) Doi, M. Explanation for the 3.4 power law of viscosity of polymeric liquids on the basis of the tube model. *J. Polym. Sci., Polym. Lett. Ed.* **1981**, *19*, 265−273.
(40) O'connor, N.; Ball, R. Confirmation of the Doi-Edwards model. *Macromolecules* **1992**, *25*, 5677−5682.
(41) Milner, S. T.; McLeish, T. C. B. Reptation and Contour-Length Fluctuations in Melts of Linear Polymers. *Phys. Rev. Lett.* **1998**, *81*, 725−728.
(42) Frischknecht, A. L.; Milner, S. T. Diffusion with Contour Length Fluctuations in Linear Polymer Melts. *Macromolecules* **2000**, *33*, 5273−5277.
(43) Leibler, L.; Rubinstein, M.; Colby, R. H. Dynamics of reversible networks. *Macromolecules* **1991**, *24*, 4701−4707.
(44) Chen, Q.; Zhang, Z.; Colby, R. H. Viscoelasticity of entangled random polystyrene ionomers. *J. Rheol.* **2016**, *60*, 1031−1040.
(45) Colby, R. H.; Zheng, X.; Rafailovich, M. H.; Sokolov, J.; Peiffer, D. G.; Schwarz, S. A.; Strzhemechny, Y.; Nguyen, D. Dynamics of Lightly Sulfonated Polystyrene Ionomers. *Phys. Rev. Lett.* **1998**, *81*, 3876−3879.
(46) Chen, Q.; Tudryn, G. J.; Colby, R. H. Ionomer dynamics and the sticky Rouse model. *J. Rheol.* **2013**, *57*, 1441−1462.
(47) Gebbie, M. A.; Valtiner, M.; Banquy, X.; Fox, E. T.; Henderson, W. A.; Israelachvili, J. N. Ionic liquids behave as dilute electrolyte solutions. *Proc. Natl. Acad. Sci. U.S.A.* **2013**, *110*, 9674−9679.
(48) Appel, M.; Fleischer, G. Investigation of the Chain Length Dependence of Self-Diffusion of Poly(dimethylsiloxane) and Poly(ethylene oxide) in the Melt with Pulsed Field Gradient NMR. *Macromolecules* **1993**, *26*, 5520−5525.
(49) Whitlow, S. J.; Wool, R. P. Diffusion of polymers at interfaces: a secondary ion mass spectroscopy study. *Macromolecules* **1991**, *24*, 5926−5938.
(50) Anderson, J. E.; Jou, J. H. Small-Angle Neutron Scattering Studies of Diffusion in Bulk Polymers: Experimental Procedures. *Macromolecules* **1987**, *20*, 1544−1549.
(51) Smith, B. A.; Samulski, E. T.; Yu, L. P.; Winnik, M. A. Polymer diffusion in molten poly(propylene oxide). *Macromolecules* **1985**, *18*, 1901−1905.
(52) Cheng, Y.; Prud'homme, R. K.; Thomas, J. L. Diffusion of Mesoscopic Probes in Aqueous Polymer Solutions Measured by Fluorescence Recovery after Photobleaching. *Macromolecules* **2002**, *35*, 8111−8121.
(53) Jourdainne, L.; Lecuyer, S.; Arntz, Y.; Picart, C.; Schaaf, P.; Senger, B.; Voegel, J.-C.; Lavalle, P.; Charitat, T. Dynamics of Poly(l-lysine) in Hyaluronic Acid/Poly(l-lysine) Multilayer Films Studied by Fluorescence Recovery after Pattern Photobleaching. *Langmuir* **2008**, *24*, 7842−7847.
(54) Pincet, F.; Adrien, V.; Yang, R.; Delacotte, J.; Rothman, J. E.; Urbach, W.; Tareste, D. FRAP to Characterize Molecular Diffusion and Interaction in Various Membrane Environments. *PLoS One* **2016**, *11*, No. e0158457.
(55) Katzenstein, J. M.; Janes, D. W.; Hocker, H. E.; Chandler, J. K.; Ellison, C. J. Nanoconfined Self-Diffusion of Poly(isobutyl methacrylate) in Films with a Thickness-Independent Glass Transition. *Macromolecules* **2012**, *45*, 1544−1552.
(56) Frank, B.; Gast, A. P.; Russell, T. P.; Brown, H. R.; Hawker, C. Polymer Mobility in Thin Films. *Macromolecules* **1996**, *29*, 6531−6534.
(57) Layman, J. M.; Borgerding, E. M.; Williams, S. R.; Heath, W. H.; Long, T. E. Synthesis and Characterization of Aliphatic Ammonium Ionenes: Aqueous Size Exclusion Chromatography for Absolute Molecular Weight Characterization. *Macromolecules* **2008**, *41*, 4635−4641.
(58) Seiffert, S.; Oppermann, W. Systematic evaluation of FRAP experiments performed in a confocal laser scanning microscope. *J. Microsc.* **2005**, *220*, 20−30.

https://doi.org/10.1021/acs.macromol.2c02388
Macromolecules 2023, 56, 3383−3392

(59) Colby, R. H.; Fetters, L. J.; Graessley, W. W. The melt viscosity-molecular weight relationship for linear polymers. *Macromolecules* **1987**, *20*, 2226−2237.
(60) Wong, L. N.; Jones, S. D.; Wood, K.; de Campo, L.; Darwish, T.; Moir, M.; Li, H.; Segalman, R. A.; Warr, G. G.; Atkin, R. Polycation radius of gyration in a polymeric ionic liquid (PIL): the PIL melt is not a theta solvent. *Phys. Chem. Chem. Phys.* **2022**, *24*, 4526−4532.
(61) Watanabe, H. Viscoelasticity and dynamics of entangled polymers. *Prog. Polym. Sci.* **1999**, *24*, 1253−1403.
(62) Pearson, D. S.; Ver Strate, G.; Von Meerwall, E.; Schilling, F. C. Viscosity and self-diffusion coefficient of linear polyethylene. *Macromolecules* **1987**, *20*, 1133−1141.
(63) Harmandaris, V. A.; Mavrantzas, V. G.; Theodorou, D. N. Atomistic Molecular Dynamics Simulation of Polydisperse Linear Polyethylene Melts. *Macromolecules* **1998**, *31*, 7934−7943.
(64) Struglinski, M. J.; Graessley, W. W. Effects of polydispersity on the linear viscoelastic properties of entangled polymers. 1. Experimental observations for binary mixtures of linear polybutadiene. *Macromolecules* **1985**, *18*, 2630−2643.
(65) Doi, M.; Graessley, W. W.; Helfand, E.; Pearson, D. S. Dynamics of polymers in polydisperse melts. *Macromolecules* **1987**, *20*, 1900−1906.
(66) Wang, Z.; Larson, R. G. Constraint Release in Entangled Binary Blends of Linear Polymers: A Molecular Dynamics Study. *Macromolecules* **2008**, *41*, 4945−4960.
(67) Peters, B. L.; Salerno, K. M.; Ge, T.; Perahia, D.; Grest, G. S. Effect of Chain Length Dispersity on the Mobility of Entangled Polymers. *Phys. Rev. Lett.* **2018**, *121*, 057802.
(68) Bulacu, M.; van der Giessen, E. Effect of bending and torsion rigidity on self-diffusion in polymer melts: A molecular-dynamics study. *J. Chem. Phys.* **2005**, *123*, 114901.
(69) Bulacu, M.; van der Giessen, E. Molecular-dynamics simulation study of the glass transition in amorphous polymers with controlled chain stiffness. *Phys. Rev. E* **2007**, *76*, 011807.
(70) von Meerwall, E.; Beckman, S.; Jang, J.; Mattice, W. L. Diffusion of liquid n-alkanes: Free-volume and density effects. *J. Chem. Phys.* **1998**, *108*, 4299−4304.
(71) Liu, H.; Paddison, S. J. Alkyl Chain Length Dependence of Backbone-to-Backbone Distance in Polymerized Ionic Liquids: An Atomistic Simulation Perspective on Scattering. *Macromolecules* **2017**, *50*, 2889−2895.
(72) Choi, U. H.; Lee, M.; Wang, S.; Liu, W.; Winey, K. I.; Gibson, H. W.; Colby, R. H. Ionic Conduction and Dielectric Response of Poly(imidazolium acrylate) Ionomers. *Macromolecules* **2012**, *45*, 3974−3985.
(73) Araque, J. C.; Hettige, J. J.; Margulis, C. J. Modern Room Temperature Ionic Liquids, a Simple Guide to Understanding Their Structure and How It May Relate to Dynamics. *J. Phys. Chem. B* **2015**, *119*, 12727−12740.

https://doi.org/10.1021/acs.macromol.2c02388
Macromolecules 2023, 56, 3383−3392